JISSE
ISSN: 2636-4425

JISSE
E-ISSN:2682-3438

Journal of International Society for Science and Engineering
Vol. 5, No. 2, 43-54 (2023)

Effect of Corrosion on Reinforced Concrete Footing Subjected to Eccentrically Loading

Ahmed Youssef [1]*, Mahmoud Hegazy Fouda [2], Hatem Mostafa [3]

[1]Associate professor, Department of Structural Engineering, Faculty of Engineering, Cairo University, Egypt

[2]Assistant professor, Department of Civil Engineering, Institute of Aviation and Engineering Technology, Giza, Egypt

[3] Professor, Department of Structural Engineering, Faculty of Engineering, Cairo University, Egypt

ARTICLE INFO

Article history:
Received:06-06-2023
Accepted:20-06-2023
Online:01-06-2023

Keywords:
Corrosion
Eccentric loading
Isolated footing
FEM
Small scale modeling

ABSTRACT

This study aims to use a small-scale model to investigate the corrosion effect on the degradation of reinforced concrete RC footings and to compare its observations with prototype-scale research results using a numerical model for footings exposed to various corrosion levels under eccentric loading. This comparison may be used to assess the efficacy of small-scale models in expressing prototype models in order to save money and time. The finite element method was used in collaboration with the ABAQUS software to study its impact on eccentric load behavior with several corrosion levels. This research also examines the influence of concrete depth on its behavior under different corrosion levels and eccentric loads with varying eccentricities. As both the corrosion ratio and the depth of the RC footing increased, the cracking pattern in the concrete became more pronounced, the extent of corrosion in the bars grew, and the difference in failure load also increased. Using the FEM, the findings will be beneficial in estimating the performance of isolated footings with corrosion damage.

1. Introduction

Wind or earthquake lateral forces can cause eccentric loads on foundations, leading to non-uniform soil pressure and moments at the footing's base. This study aims to investigate the effect of eccentric loads on footings with different degrees of corrosion. If the eccentricity (e) of the load is small ($e \leq L/6$, where L is the length in the longitudinal direction), compression stresses develop over the footing-soil contact. The maximum bearing capacity should be compared to the highest stress (fmax) to determine the footing's stability. The difference between the maximum stress (fmax) and minimum stress (fmin) decreases as the eccentricity of the load increases until it reaches a limit of $e = L/6$. At this point, fmin becomes zero. If the eccentricity is further increased, tensile stress will occur. When the eccentricity exceeds L/6, a triangular stress distribution appears over a section of the base [1]. Steel bar corrosion is a main source of durability loss in reinforced concrete constructions that are subjected to chloride in coastal areas [2-4]. The area losses of steel bars reduced the load bearing capacity of RC elements and the bond strength between corroded steel and concrete, resulting in losses in the confinement provided by exposed transverse reinforcement and changes in steel mechanical properties [5-17]. RC footings stuffers against corrosion attacks are in salt-prone and coastal areas. As far as we know, the behavior of RC footing with several corrosion levels under eccentric loading hasn't been investigated by any researchers compared with other RC members such as columns, slabs, and beams. Therefore, this study focuses on investigating the behavior of isolated footings under eccentric loading and varying levels of corrosion.

The present study employs numerical parametric analysis to investigate the effects of varying concrete depths on the response of reinforced concrete footings subjected to eccentric loading and varying corrosion levels at both small and prototype scales. The obtained numerical results will be utilized to develop an analytical method for assessing the different failure modes related to the eccentric load bearing capacity. Furthermore, a comparative analysis will be performed between the results of small-scale and prototype-scale modeling to evaluate the suitability of small-scale models in predicting the behavior of prototype-scale footings.

2. Numerical validation model

2.1. Numerical model properties

* Ahmed Youssef, Associate Professor, Structural Engineering Department, Faculty of Engineering, Cairo University, Cairo, Egypt, +201273001615, ahmedyoussef@cu.edu.eg

In the present study, corrosion damage assessment was conducted using the model of concrete damage plasticity (CDP) with the aid of the ABAQUS software [6]. Uniaxial stress was applied to the concrete and its parameters were identified to investigate their influence under compound stress, as listed in Table 1. Furthermore, the mechanical properties of the concrete, such as the modulus of elasticity and Poisson's ratio, were defined and are presented in Table 2.

Table 1: The concrete damage plasticity CDP models parameter.

Parameter	Dilation angle	Eccentricity angle	f_b/f_c	K	Viscosity parameter
Value	40	0.1	1.16	0.667	0

Table 2: Elastic properties of concrete, steel bar, and sand

Material properties	Modulus of elasticity [N/mm^2]	Poisson's ratio
concrete	33345.76	0.2
Steel bar	2100000	0.3
Corrosion bars with corrosion ratio% @ 4.21 %-9.11 %	120000 [8]	0.45 (assumed)
Corrosion bars with corrosion ratio% @ 24.56 %	60000 (assumed)	0.45 (assumed)
Corrosion bars with corrosion ratio% @ 30.67 %	50000 (assumed)	0.45 (assumed)
Medium dense sand	15	0.35

In this research, the ABAQUS finite element software was employed to simulate the nonlinear behavior of reinforced concrete subjected to corrosion of steel bars [9]. The concrete and steel bars were discretized using solid and wire elements, respectively. The concrete behavior at the nonlinear stage was represented by the damaged plasticity concrete CDP model, whereas the steel reinforcement was modeled by the plastic/isotropic model. The corrosion effect was analyzed in terms of the reduction of the cross-sectional area of the reinforcement bars, the decrease of the bond strength between the steel reinforcement and concrete, and the alteration of the steel mechanical properties, such as the modulus of elasticity and Poisson's ratio, according to Table 2. To simulate the slippage between the steel bars and concrete, an ABAQUS embedded region constraint was employed, which assumes a strain compatibility or complete connection between the steel and concrete. However, this approach is not sufficient to capture the crucial decrease of the steel reinforcement-concrete connection during corrosion. Therefore, a new approach should be developed to simulate the interaction between steel reinforcement and concrete under corrosion. The corrosion expansion coefficient was assumed to be 3. The corrosion-induced expansion of the steel volume leads to the cracking of concrete, which can propagate to the surface due to the increased pressure. [8].

2.2. Validation model and results

The authors conducted experimental tests on five small-scale models, with dimensions of 250 x 250 x 40 mm and a 40 x 40 mm column as a 1/8 scale down. The models were cast with concrete having a characteristic strength of f_{cu} = 40 MPa and longitudinal reinforcement with yield stress fy equal to 850 MPa. The main reinforcement bars of the footing were 7ϕ2 in both directions. The small models were subjected to an accelerated corrosion process using the constant current method to induce four different levels of corrosion: Sp 4.21, Sp 9.11, Sp 24.56, and Sp 30.67. (Here, Sp 4.21 indicates a specimen with a corrosion ratio of 4.21% loss from the steel bar mass.)

The envelope curves of the axial load-displacement responses of all small-size models are shown in fig.1. It illustrates the difference between the experimental and numerical results. The relation between axial load bearing capacity and displacement in the center of the footing under centric force for corroded footing subjected to concentrated load; it is observed that significant degradation of stiffness and loading failure compared with the control footing Sp 0. The deformation continues to increase even as the load decreases after the maximum force is reached due to the plasticization that occurs in the concrete. The failure load experimentally for Sp 0 control footing was 42.6 kN while the failure loads for corroded footings Sp 4.21, Sp 9.11, Sp 24.56, and Sp 30.67 were 35.4, 34.3, 26.9, 22.9 kN respectively, note that the Sp 4.21 is the specimen have 4.21 % corrosion ratio. While the numerical results for the relation between axial load bearing capacity and displacement for corroded footing subjected to axial load also found that significant degradation of stiffness and failure load is observed compared with the control footing. The failure load numerically for Sp 0 control footing was 40.2 kN while the failure loads for corroded footing Sp 4.21, Sp 9.11, Sp 24.56, and Sp 30.67 were 33.6, 32.9, 28.6, 24.7 kN respectively.

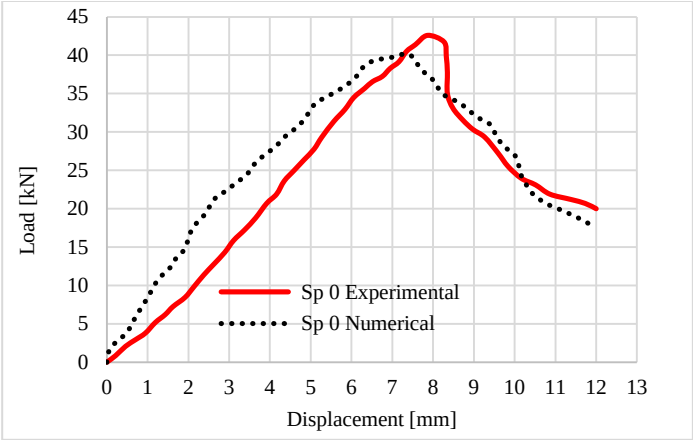

a) Sp 0

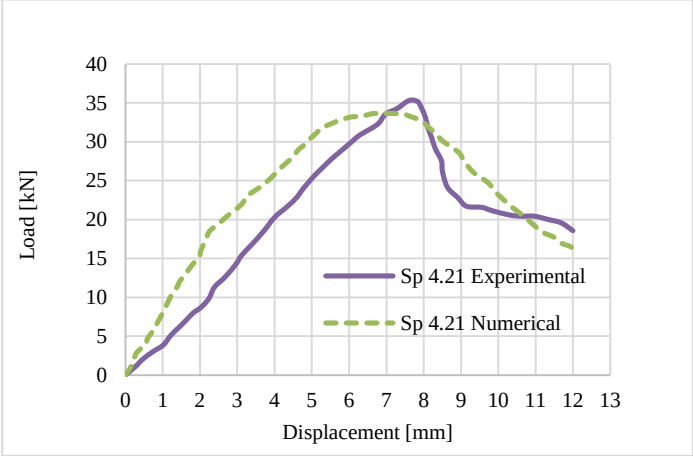

b) Sp 4.21

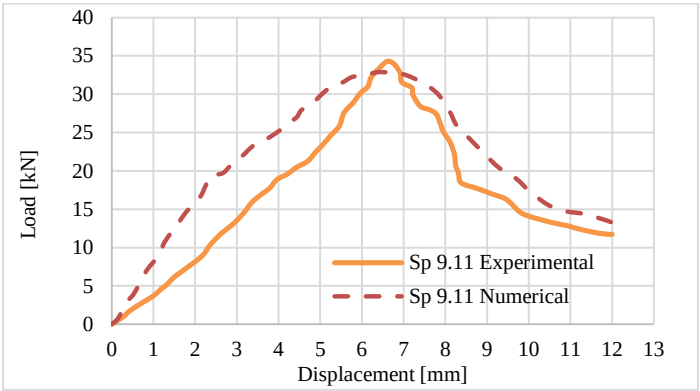

c) Sp 9.11

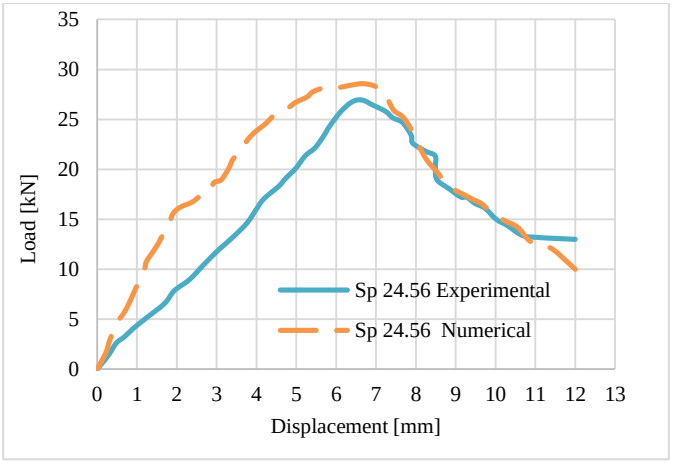

d) Sp 24.56

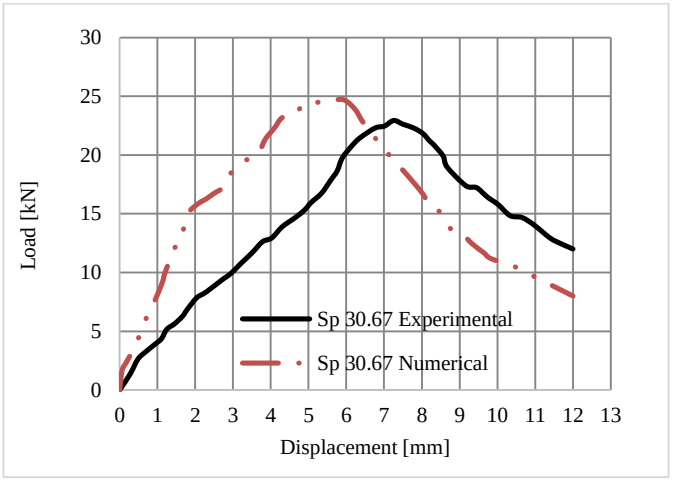

e) Sp 30.67

Fig. 1: Experimental and numerical envelope curves:

a) Sp 0, b) Sp 4.21, c) Sp 9.11, d) Sp 24.56, e) Sp 30.67

Fig. 1 illustrates the results of experimental and numerical specimens for the relation between failure load and displacement for corroded footing subjected to axial load; it also finds a slight difference at the beginning of the slope in the relation between load and displacement, but it follows the same behavior. The displacement was measured from the top point of the column under the loading cell. The difference between the FEM and the experimental results was found to be close to each other with an acceptable ratio. The average variation of ultimate load (experimental and by FEM) for small-scale was found to be less than 5.6 %, and the average deflection variation was 6.8 %. Also, Fig. 2. Represent the relation between corrosion ratio % and the reduction in failure load-bearing capacity as a ratio from the control footing.

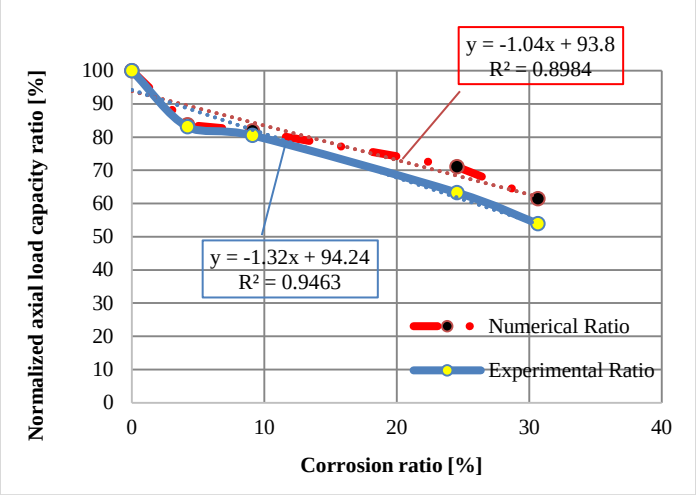

Fig. 2: Corrosion ratio [%] and axial load capacity [%].

3. Parametric study

For small-scale modeling, numerical analysis was carried out on twenty small-scale 1/8 RC isolated footing models. Footings were divided into four series A, B, C, and D as shown in Table 3.

- Series A is isolated footing with 250x250x40 mm with different levels of corrosion Sp 0, Sp 4.21, Sp 9.11, Sp 24.56, and Sp 30.67 was subjected to axial load with eccentricity e = 0 as shown in previous section numerical validation.
- series B is isolated footing with 250x250x40 mm with different levels of corrosion Sp 0, Sp 4.21, Sp 9.11, Sp 24.56, and Sp 30.67 was subjected to small eccentric loading with eccentricity e < L/6 (i.e, e = 18.75 mm).
- series C is isolated footing with 250x250x40 mm with different levels of corrosion Sp 0, Sp 4.21, Sp 9.11, Sp 24.56, and Sp 30.67 was subjected to eccentric loading with eccentricity e = L/6 (i.e, e = 41.67 mm).
- series D is isolated footing with 250x250x40 mm with different levels of corrosion Sp 0, Sp 4.21, Sp 9.11, Sp 24.56, and Sp 30.67 was subjected to big eccentrical loading with eccentricity e > L/6 (i.e, e = 56.25 mm).

Note that: The dimensions and level of corrosion are the same for all, only the eccentricity changes.

Table 3: small scale modeling description.

Small scale 1/8	**250x250x40 mm 7 ϕ 2 at both directions**	**Series A**	**e = 0**	**All models were tested under 5 different corrosion levels Sp 0 Sp 4.21 Sp 9.11 Sp 24.56 Sp 30.67**
		Series B	**e < L/6 = 18.75 mm**	
		Series C	**e = L/6 = 41.67 mm**	
		Series D	**e > L/6 = 56.25 mm**	

Where: (* e: eccentricity, * L: length of longitudinal direction)

For prototype modeling, numerical analysis was conducted on sixty RC isolated footing models, which were divided into three series based on concrete depth and eccentricity, as outlined in Table 4. Each series featured isolated footings with dimensions of 2000x2000 mm and levels of corrosion Sp 0, Sp 4.21, Sp 9.11, Sp 24.56, and Sp 30.67. The footings were subjected to axial loading with eccentricity e = 0, e < L/6 = 150 mm, e = L/6 = 333.3 mm, and e > L/6 = 450 mm.

The concrete depth varied across the series, with depths of 300, 400, and 500 mm tested. The minimum depth of 300 mm was chosen as the prototype modeling scale 1 according to the Egyptian Code [10], which mandates that the least dimension of concrete depth for RC footing is the largest form 300 mm or less dimension from column dimension. The clear concrete cover had a thickness of 50 mm, and the column was 300x300 mm with a height of 1000 mm.

The soil was simulated using solid circular parts measuring 5000 mm in diameter and 2500 mm in height. Thirteen 12 mm diameter steel bars were used as longitudinal reinforcement in each direction, with a yield stress of 500 N/mm2.

Table 4: Prototype scale modeling description.

Prototype scale with different RC depth	**Scale 1 2000x2000x300 mm**	Series E	• $e = 0$ • $e < L/6 = 150$ mm • $e = L/6 = 333.3$ mm • $e > L/6 = 450$ mm Where: e: eccentricity, L: length of longitudinal direction	All models were tested under 5 different corrosion levels • Sp 0 • Sp 4.21 • Sp 9.11 • Sp 24.56 • Sp 30.67
		Series F		
		Series G		
		Series H		
	2000x2000x400 mm	Series I		
		Series J		
		Series K		
		Series L		
	2000x2000x500 mm	Series M		
		Series N		
		Series O		
		Series P		

4. Material properties

4.1. Small-scale modeling

The analyzed footings were assumed to have a characteristic strength of f_{cu} = 40 MPa. Besides, the longitudinal reinforcement was assumed to have yield stresses equal to 850 Mpa. For the analyzed footings, the main reinforcement area of the footing as is 7ϕ2 in both directions. The soil properties were defined as elastic material young's modulus and passion ratio as outlined in Table 2

4.2. Prototype modeling

The analyzed footings were assumed to have a characteristic strength of fcu = 40 MPa and its concrete tensile rupture $f_{ctr} = 0.6\sqrt{f_{cu}}$ = 3.78 MPa as recommended by the Egyptian Code of Practice (ECP-203) [10]. Besides, the longitudinal reinforcement was assumed to have yield stresses equal to 500 MPa. For the analyzed footings, the main reinforcement area of the footing as is 13 ϕ 12 in both directions. The soil properties were defined as elastic material young's modulus and passion ratio as outlined in Table 2. Additionally, the elastic properties of the concrete and sand materials used in the study were considered.

5. Mesh sensitivity

To ensure accurate results and reduce computational time, we experimented with various mesh sizes, adapting the dimensions of the mesh to minimize stress concentration areas, as illustrated in Fig. 3. Each part was meshed separately and assigned the corresponding section, with a four-node doubly curved general-purpose shell featuring finite membrane strains used for the concrete, and a truss element T3D2 used for the rebar. To ensure optimal accuracy, the slave surface mesh was refined compared to the master surface. The mesh size for the small-scale footing and steel mesh for longitudinal reinforced bars was set to 5 mm, while for other elements, it was 10 mm. In the prototype scale, the mesh size was increased to 50 mm for both the footing and reinforced steel.

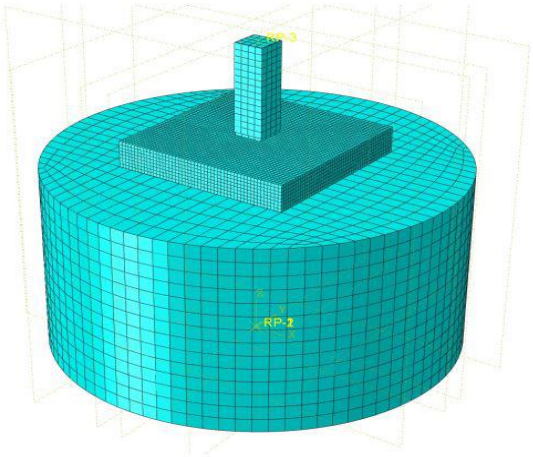

Fig. 3: Meshed elements.

6. Numerical result and discussion

6.1. Small scale 1/8 result and discussion

The reinforced concrete footing with different steel corrosion levels was tested using non-linear analysis using ABAQUS. Fig. 4. represents the relationship between corrosion ratio % and eccentric loading capacity reduction as a ratio from the control specimen for small-scale footing with different eccentricity e = 0, e < L/6, e = L/6, and e > L/6.

The envelope curves in Fig. 5 depict the load-displacement response of all specimens. The numerical results show a clear correlation between the load bearing capacity and displacement in the center of the footing under eccentric force

for small-scale corroded footings with different eccentricity e. There is a significant degradation of loading capacity and stiffness with respect to the failure load and stiffness of the control footing. Table 5 presents the values of failure load and displacement in the center of the footing under eccentric force for all small-scale specimens with eccentricity, which clearly demonstrate the relationship between the reduction in failure load with respect to the control footing and the corrosion ratio % for different eccentricity values.

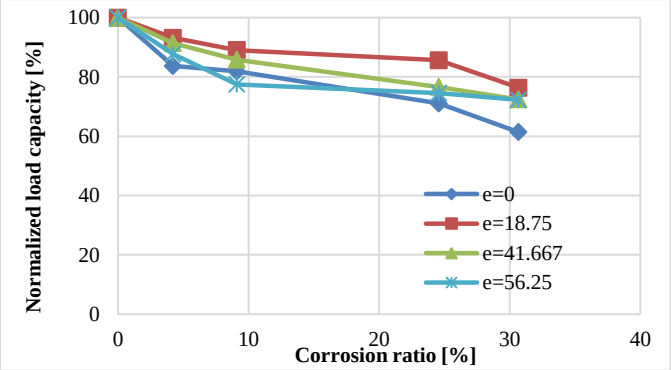

Fig. 4: Relationship between corrosion ratio [%] and load capacity reduction as a ratio from the control specimen for small footings

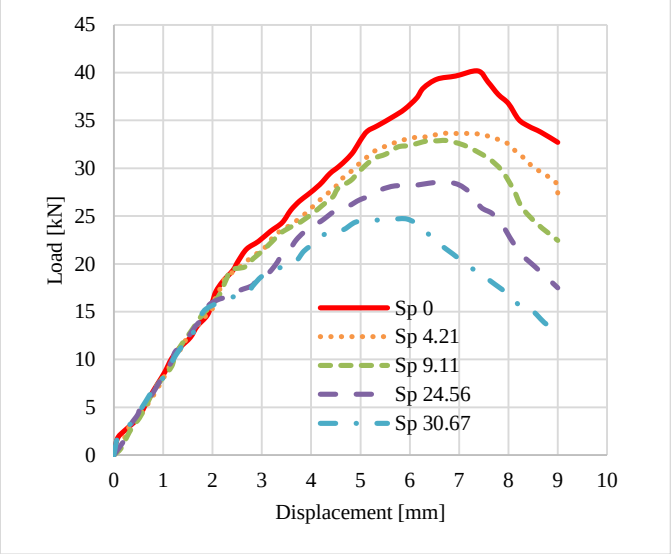

a) e = 0 mm

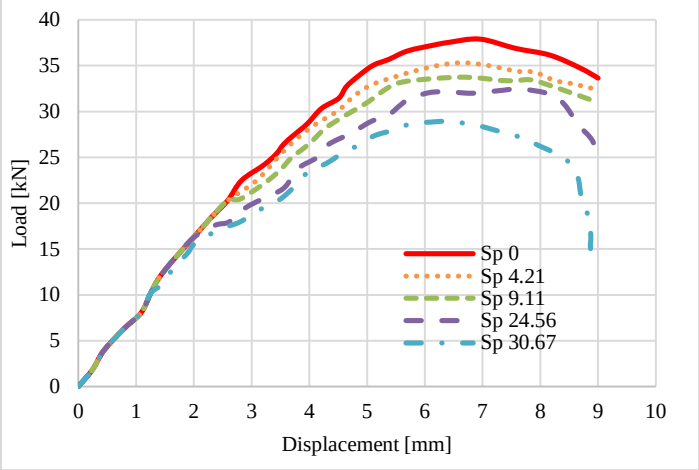

b) Small eccentricity e < L/6 = 18.75 mm

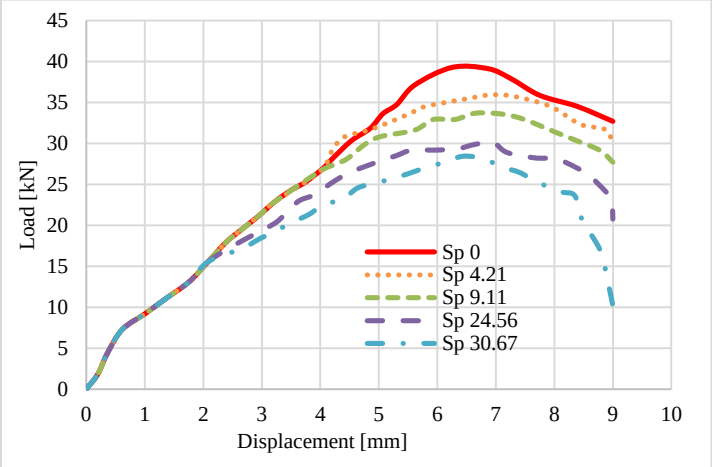

c) Eccentricity e = L/6 = 41.667 mm

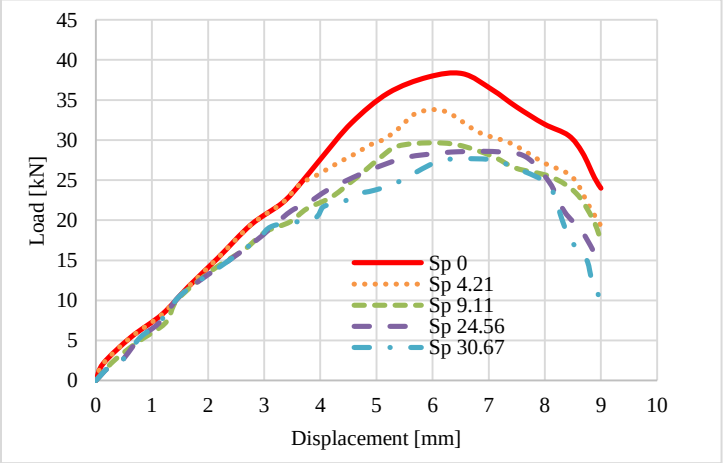

d) Big eccentricity e > L/6 = 56.25 mm

Fig. 5: Numerical envelope curve of all small-scale specimens with eccentricity: a) e = 0 mm, b) small eccentricity e < L/6 = 18.75 mm, c) eccentricity e = L/6 = 41.667 mm, d) big eccentricity e > L/6 = 56.25 mm.

Table 5: Illustrate numerical results for all small-scale specimens with eccentricity.

Seires	*Corrosion ratio [%]*	*Numerical results for small scale*		
		Displacement [mm]	*Load [kN]*	*Axial load capacity ratio [%]*
Seires A e = 0	*Sp 0*	*7.38*	*40.2*	*100*
	Sp 4.21	*7.22*	*33.6*	*83.5*
	Sp 9.11	*6.76*	*32.9*	*81.8*
	Sp 24.56	*6.73*	*28.6*	*71*
	Sp 30.67	*5.95*	*24.7*	*61.4*
Seires B e < L/6	*Sp 0*	*6.95*	*37.89*	*100*
	Sp 4.21	*6.68*	*35.31*	*93.2*
	Sp 9.11	*6.6*	*33.74*	*89*
	Sp 24.56	*7.65*	*32.45*	*85.6*
	Sp 30.67	*6.4*	*28.94*	*76.4*
Seires C e = L/6	*Sp 0*	*6.25*	*39.27*	*100*
	Sp 4.21	*6.9*	*35.9*	*91.4*
	Sp 9.11	*6.67*	*33.69*	*85.8*
	Sp 24.56	*6.96*	*30.1*	*76.6*
	Sp 30.67	*6.45*	*28.44*	*72.4*
Seires D e > L/6	*Sp 0*	*6.54*	*38.57*	*100*
	Sp 4.21	*6.23*	*33.57*	*87.7*
	Sp 9.11	*5.95*	*29.66*	*77.5*
	Sp 24.56	*6.46*	*28.54*	*74.6*
	Sp 30.67	*6.52*	*27.66*	*72.3*

6.2. Prototype scale 1 t=300 mm results and discussion

The tests showed that under eccentric loading for reinforced concrete isolated footings with different steel corrosion levels were tested using non-linear analysis using FEM. Fig. 6. Represent the relationship between corrosion ratio % and eccentric loading capacity reduction as a ratio from the control specimen for prototype –scale 1 footing with different eccentricity e = 0, e < L/6, e = L/6, and e > L/6.

The envelope curves of the load-displacement response of all specimens with 2000x2000x300 mm dimension as a prototype scale 1 are shown in Fig. 7. It illustrates the numerical results for the relation between load bearing capacity and displacement in the center of the footing under centric force for corroded footing subjected to eccentric load with different eccentricity, significant degradation of loading capacity and stiffness with respect to the failure load, and stiffness of the control footing. Table 6 illustrates the value of failure load for the numerical results and explains the relationship between the reductions in failure load with respect control footing with the corrosion ratio % with respect to different eccentricity.

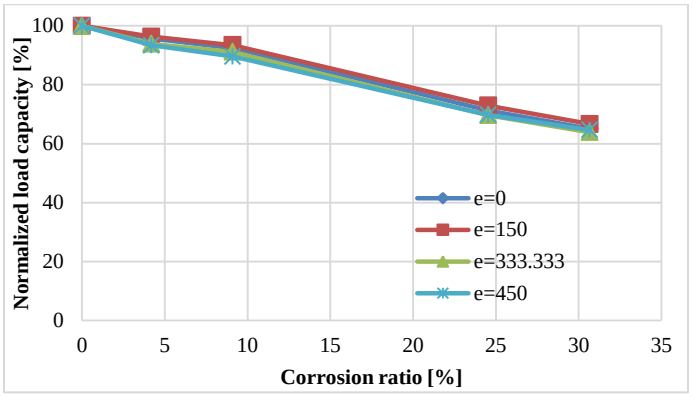

Fig. 6: Relationship between corrosion ratio [%] and load capacity reduction as a ratio from the control specimen for prototype scale 1 footings t = 300 mm.

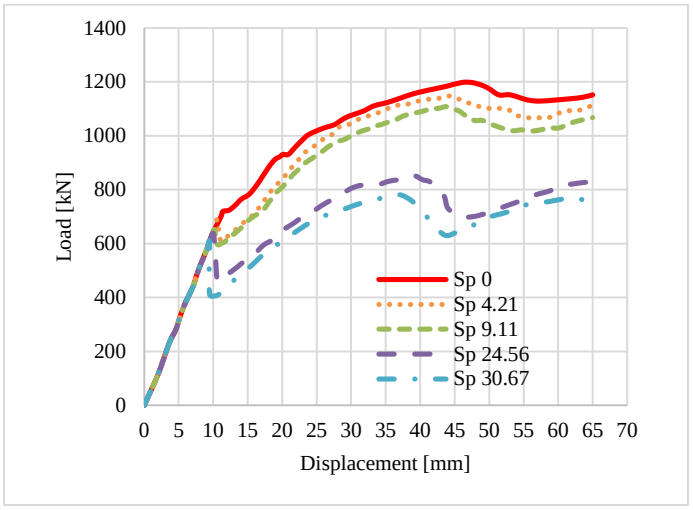

a) e = 0 mm

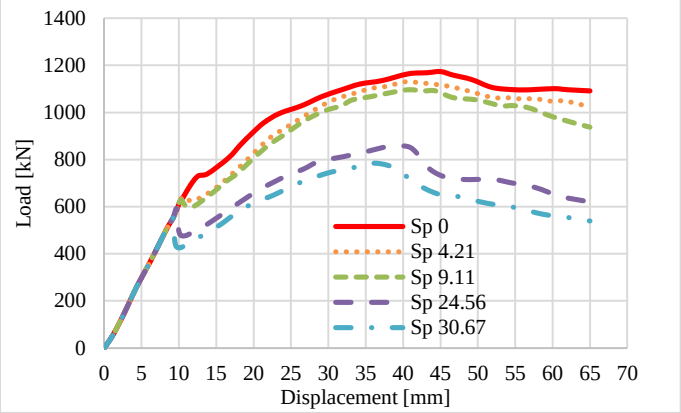

b) Small eccentricity e < L/6 = 150 mm

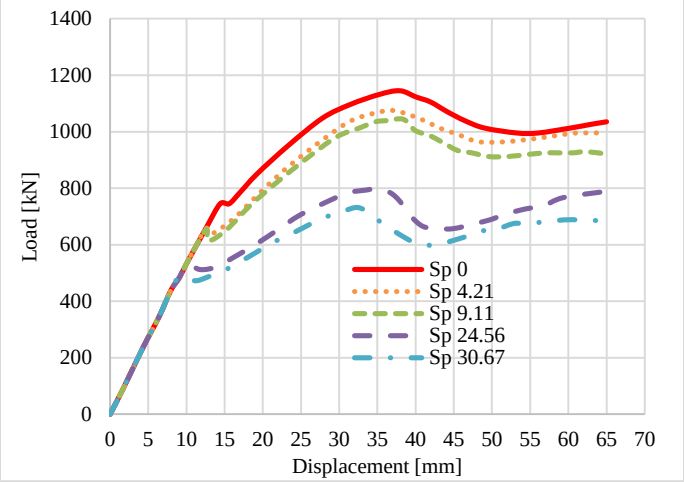

c) Eccentricity e = L/6=333 mm

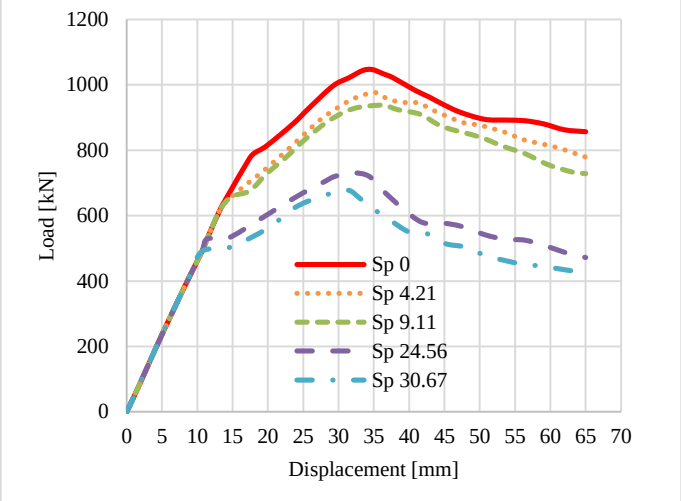

d) Big eccentricity e > L/6=450 mm

Fig. 7: Numerical envelope curves of all prototype scale, t = 300 mm specimens with eccentricity: a) e = 0 mm, b) small eccentricity e < L/6 = 150 mm, c) eccentricity e = L/6 = 333 mm, d) big eccentricity e > L/6 = 450 mm.

Table 6: Illustrate Numerical results for all prototype-scale t = 300 mm specimens with eccentricity.

Seires	*Corrosion ratio [%]*	*Numerical results for prototype scale t = 300 mm*		
		Displacement [mm]	*Load [kN]*	*Axial load capacity ratio [%]*
Seires E e = 0	*Sp 0*	*46.02*	*1198*	*100*
	Sp 4.21	*43.65*	*1147*	*95.74*
	Sp 9.11	*43.74*	*1108*	*92.48*
	Sp 24.56	*39.02*	*853*	*71.2*
	Sp 30.67	*35.87*	*780*	*65.1*
Seires F e < L/6	*Sp 0*	*45*	*1173.5*	*100*
	Sp 4.21	*40.3*	*1130.1*	*96.3*
	Sp 9.11	*40.8*	*1096.4*	*93.4*
	Sp 24.56	*38*	*855.4*	*72.9*
	Sp 30.67	*37.8*	*782.17*	*66.7*
Seires G e = L/6	*Sp 0*	*37.9*	*1145*	*100*
	Sp 4.21	*37.2*	*1074.7*	*93.9*
	Sp 9.11	*38.4*	*1044*	*91.2*
	Sp 24.56	*34.8*	*797.8*	*69.7*
	Sp 30.67	*32.4*	*731.8*	*63.9*
Seires H e > L/6	*Sp 0*	*34.8*	*1046.8*	*100*
	Sp 4.21	*35*	*976.6*	*93.4*
	Sp 9.11	*34.9*	*937.5*	*89.6*
	Sp 24.56	*32.1*	*730.5*	*69.8*
	Sp 30.67	*31.6*	*676.5*	*64.6*

6.3. Prototype scale t=400 mm results and discussion

The use of non-linear FEM analysis on reinforced concrete isolated footings under eccentric loading, with varying levels of steel corrosion, has established a strong correlation between corrosion ratio and reduction in eccentric loading capacity. Fig. 8 provides a visual representation of this relationship for prototype-scale footings with different eccentricities. The load-displacement response envelope curves for all specimens, each with dimensions of 2000x2000x400 mm as a prototype, are shown in Fig. 9, and clearly demonstrate the detrimental effects of corrosion on load-bearing capacity and stiffness of the footings under eccentric loading, in comparison to the failure load and stiffness of the control footing.

Displacement measurements were taken at the center of the footing under centric force. Table 7 details numerical values for the failure load and explains the correlation between reduction in failure load and corrosion ratio for different eccentricities relative to the control footing.

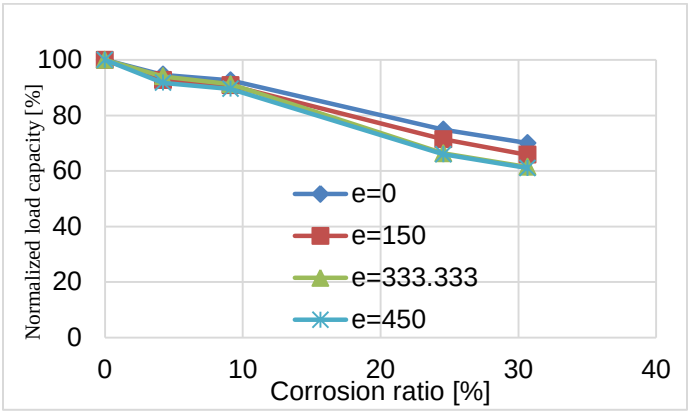

Fig. 8: Relationship between corrosion ratio [%] and load capacity reduction as a ratio from the control specimen for prototype scale footings t = 400 mm.

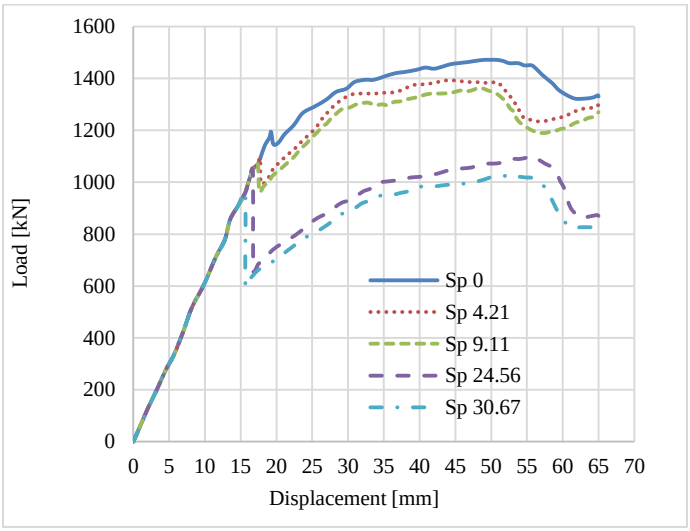

a) e = 0 mm

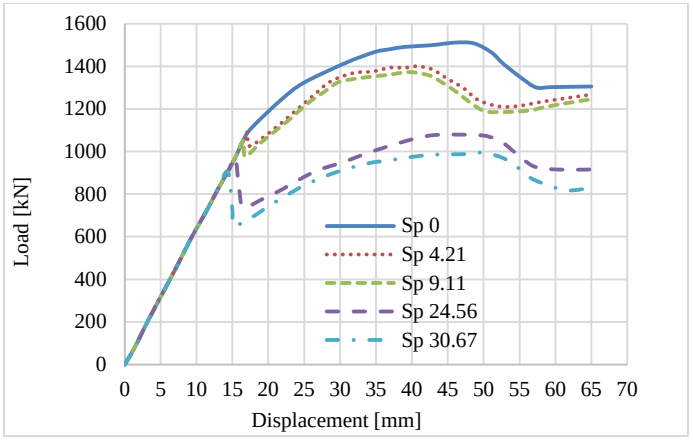

b) Small eccentricity e < L/6 = 150 mm

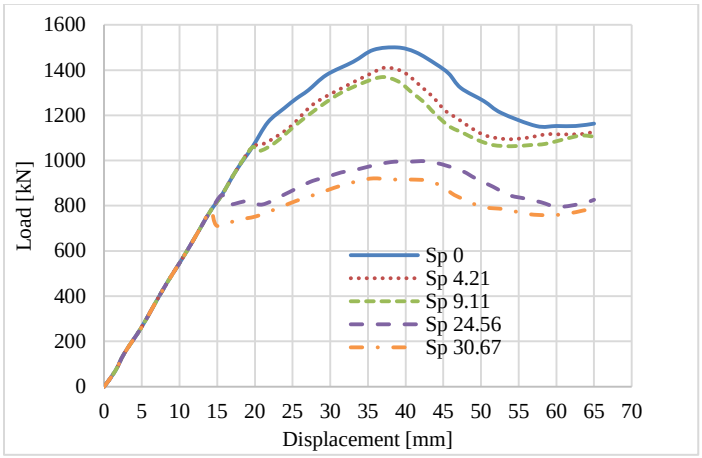

c) Eccentricity e = L/6 = 333 mm

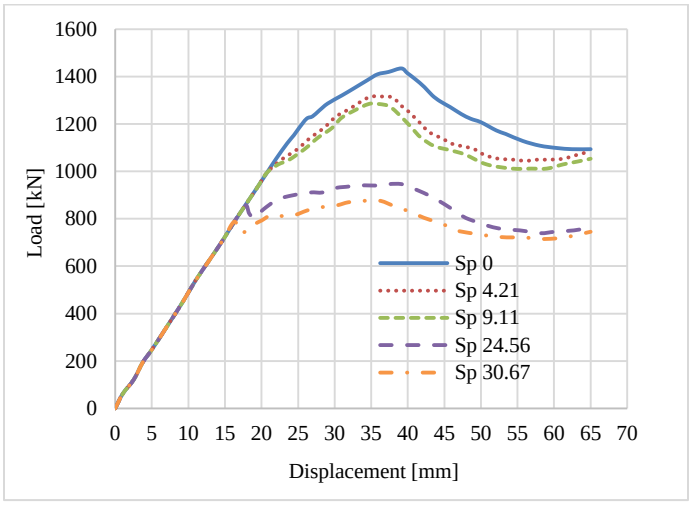

d) Big eccentricity e > L/6 = 450 mm

Fig. 9: Numerical envelope curve of all prototype scale t = 400 mm specimens with eccentricity: a) e = 0 mm, b) small eccentricity e < L/6 = 150 mm, c) eccentricity e = L/6 = 333 mm, d) big eccentricity e > L/6 = 450 mm.

Table 7: Illustrate numerical results for all prototype-scale t = 400 mm specimens with eccentricity.

Series	*Corrosion ratio [%]*	*Numerical results for prototype scale t = 400 mm*		
		Displacement [mm]	*Load [kN]*	*Axial load capacity ratio [%]*
Seires I e = 0	*Sp 0*	*50.7*	*1472*	*100*
	Sp 4.21	*45.3*	*1392*	*94.6*
	Sp 9.11	*48.7*	*1363*	*92.6*
	Sp 24.56	*55.7*	*1101*	*74.8*
	Sp 30.67	*52.4*	*1030*	*69.9*
Seires J e < L/6	*Sp 0*	*46*	*1511.3*	*100*
	Sp 4.21	*40.8*	*1400.4*	*92.7*
	Sp 9.11	*39.7*	*1372.8*	*90.8*
	Sp 24.56	*46.7*	*1079.2*	*71.4*
	Sp 30.67	*49.9*	*994.5*	*65.8*
Seires K e = L/6	*Sp 0*	*38.9*	*1500*	*100*
	Sp 4.21	*37.2*	*1410.5*	*94*
	Sp 9.11	*36.7*	*1368.4*	*91.2*
	Sp 24.56	*38.5*	*994.7*	*66.3*
	Sp 30.67	*35.7*	*921.1*	*61.4*
Seires L e > L/6	*Sp 0*	*39.1*	*1434.6*	*100*
	Sp 4.21	*35.1*	*1316.1*	*91.7*
	Sp 9.11	*34.6*	*1284.4*	*89.5*
	Sp 24.56	*37.5*	*946.7*	*65.9*
	Sp 30.67	*33.6*	*875.6*	*61*

6.4. Prototype scale t=500 mm results and discussion

The performance of reinforced concrete footings under eccentric loading was tested using non-linear FEM analysis with varying levels of steel corrosion. The results are presented in Fig.10, which shows the relationship between the corrosion ratio percentage and the reduction in eccentric loading capacity expressed as a ratio from the control specimen for prototype-scale footings with different eccentricities. Fig.11 shows the load-displacement response envelope curves for all specimens with dimensions of 2000x2000x500 mm as a prototype, indicating the relationship between load bearing capacity and displacement in the center of the footing under centric force for corroded footings subjected to eccentric loads with varying eccentricities. The findings show a significant degradation in loading capacity and stiffness in comparison to the failure load and stiffness of the control footing. Table 8 provides numerical values for the failure load and explains the correlation between the reduction in failure load and the corrosion ratio for different eccentricities relative to the control footing. The results emphasize the importance of considering the impact of steel corrosion on the performance of reinforced concrete footings under eccentric loading conditions.

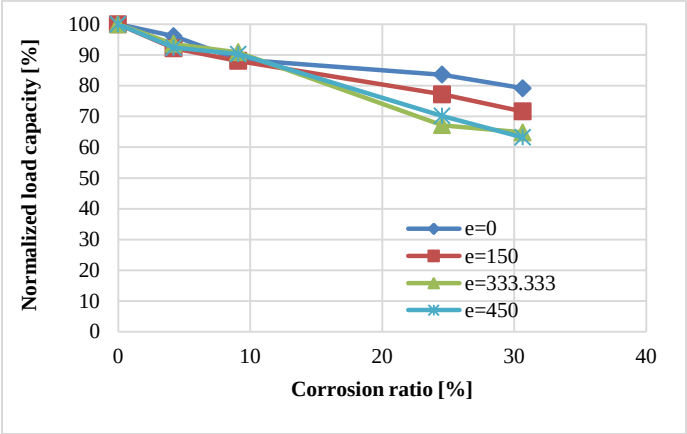

Fig. 10: Relationship between corrosion ratio [%] and load capacity reduction as a ratio from the control specimen for prototype scale footings t = 500 mm.

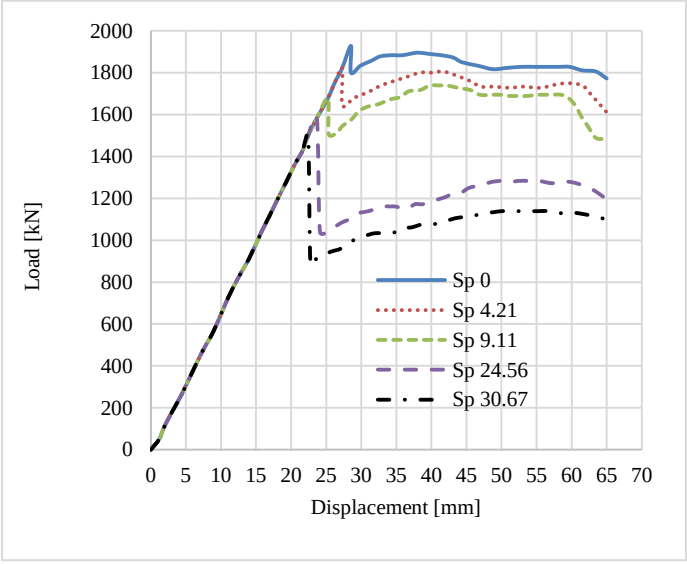

a) e = 0 mm

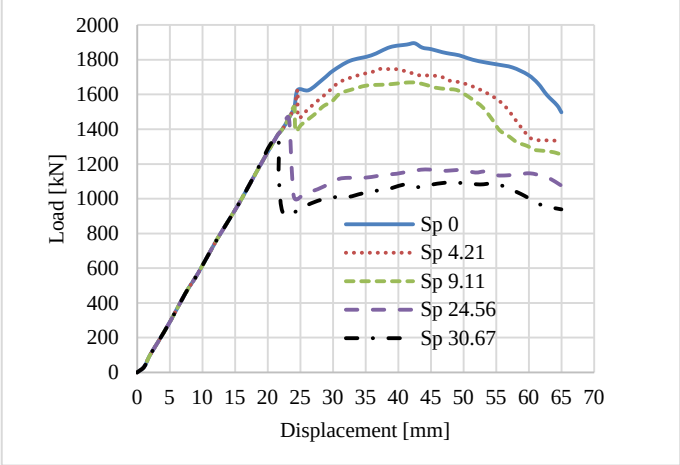

b) Small eccentricity e < L/6 = 150 mm

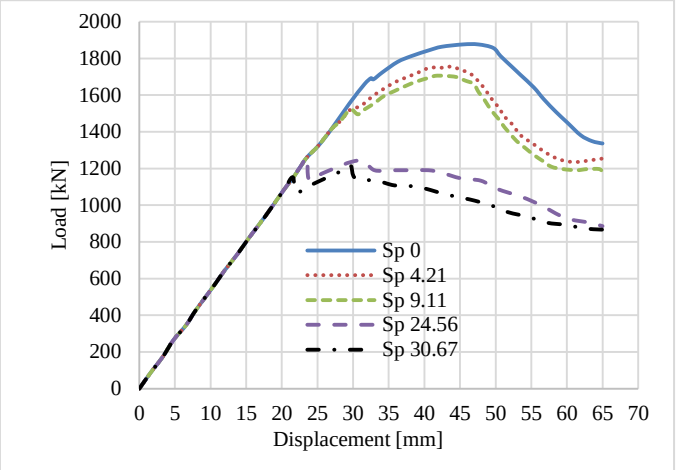

c) Eccentricity e = L/6 = 333 mm

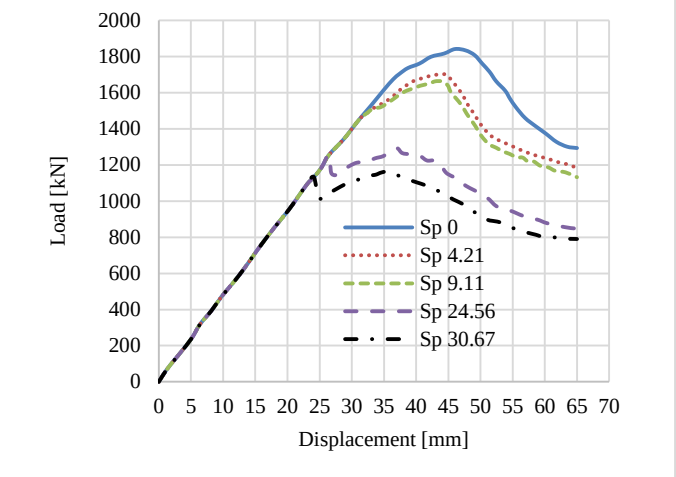

d) Big eccentricity e > L/6 = 450 mm

Fig. 11: Numerical envelope curve of all prototype scale t = 500 mm specimens with eccentricity: a) e = 0 mm, b) small eccentricity e < L/6 = 150 mm, c) eccentricity e = L/6 = 333 mm, d) big eccentricity e > L/6 = 450 mm.

Table 8: Illustrate numerical results for all prototype-scale t = 500 mm specimens with eccentricity.

Series	*Corrosion ratio [%]*	*Numerical results for prototype scale t = 500 mm*		
		Displacement [mm]	*Load [kN]*	*Axial load capacity ratio [%]*
Seires M e = 0	*Sp 0*	*38.5*	*1895*	*100*
	Sp 4.21	*27.3*	*1822*	*96.1*
	Sp 9.11	*25.3*	*1678*	*88.5*
	Sp 24.56	*23.7*	*1584*	*83.6*
	Sp 30.67	*22.4*	*1500*	*79.2*
Seires N e < L/6	*Sp 0*	*42.5*	*1894.8*	*100*
	Sp 4.21	*37.1*	*1746.7*	*92.2*
	Sp 9.11	*41.3*	*1668.7*	*88.1*
	Sp 24.56	*23.2*	*1462.7*	*77.2*
	Sp 30.67	*21.4*	*1357.2*	*71.6*
Seires O e = L/6	*Sp 0*	*45.4*	*1876.2*	*100*
	Sp 4.21	*43.8*	*1755.6*	*93.6*
	Sp 9.11	*41.5*	*1704.8*	*90.8*
	Sp 24.56	*23.5*	*1260.3*	*67.2*
	Sp 30.67	*29.6*	*1215.9*	*64.8*
Seires P e > L/6	*Sp 0*	*46*	*1841.3*	*100*
	Sp 4.21	*43.7*	*1700.8*	*92.4*
	Sp 9.11	*42.9*	*1662.6*	*90.3*
	Sp 24.56	*37.1*	*1292.2*	*70.2*
	Sp 30.67	*35.7*	*1164*	*63.2*

7. Conclusions

This study aimed to assess the efficacy of small-scale models in expressing prototype models and also to examine the effect of eccentric loading with different eccentricities and increasing concrete depths on the behavior of isolated footing exposed to several corrosion levels by FEM using ABAQUS to estimate the performance of isolated footings with corrosion damage.

It can be concluded that:

- It is observed that significant degradation of stiffness and loading failure compared with the control footing.

- The corroded steel expansion model is a reliable method for modeling corrosion damage in isolated reinforced concrete footings.
- The elastic behavior of the RC isolated footing modeled by FEM was stiffer than that of the experimental footing.
- It was found that the difference between small-scale and prototype models for axial loading e = 0 was 5.8 %, small eccentricity e < L/6 was 6.9 %, eccentricity e = L/6 was 4.5 %, and big eccentricity e > L/6 was 1.4 %.
- It was found that using of small scale applies to representing prototype models.
- The reduction in ultimate load increases with higher corrosion levels at the same depth.
- Prototype cases illustrate that with a high corrosion ratio, the reduction in ultimate load is reduced with greater depths at the same eccentricity.

These findings emphasize the importance of considering the effects of corrosion damage and eccentric loading in the design and maintenance of reinforced concrete footings. The use of small-scale models can provide a cost-effective and reliable method for evaluating the behavior of prototype models. Further research is needed to extend the findings of this study to a broader range of scenarios and practical applications.

References

[1] GHONEIM, M. - EL-MIHILMY, M.: Design of Reinforced Concrete Structures. Book, Vol. 3, 1st edition, 2011.

[2] XIAO YAN - HAITAO YU: Numerical Simulation of Hydraulic Fracturing with Consideration of the Pore Pressure Distribution Based on the Unified Pipe-Interface Element Model. Engineering Fracture Mechanics, Vol. 275, 2022, https://doi.org/10.1016/j.engfracmech.2022.108836.

[3] YE, H. - FU, C. - TIAN, Y. - JIN, N.: Chloride-Induced Steel Corrosion in Concrete under Service Loads. Springer Singapore, 2020.

[4] ZHIGANG SHAN - SHANSUO ZHENG - HAO ZHENG - YALIN LI - JINQI DONG: Seismic Behavior and Damage Evolution of Corroded RC Columns Designed for Bending Failure in an Artificial Climate. Structures, Vol. 38, 2022, p. 184-201, https://doi.org/10.1016/j.istruc.2022.01.072.

[5] YING MA - YI CHE - JINXIN GONG: Behavior of Corrosion Damaged Circular Reinforced Concrete Columns under Cyclic Loading, https://doi.org/10.1016/j.conbuildmat.2011.11.002.

[6] ABAQUS, Abaqus6.14, Abaqus 6.14 analysis user's Guide, p. 14, 2014.

[7] FATEN Y. TAQI - MOHAMMED A. MASHREI - HAYDER M. OLEIWI: Numerical Analysis of Corrosion Reinforcements in Fibrous Concrete Beams. Civil and Environmental Engineering, Vol. 17, Iss. 1, 2021, pp. 259-269, https://doi.org/10.2478/cee-2021-0027.

[8] GERMAN, M. - PAMIN, J.: FEM Simulations of Cracking in RC Beams due to Corrosion Progress. Behavior Arch Civ Mech Eng, Vol. 15, Iss. 4, 2015, pp. 1160–72, http://dx.doi.org/10.1016/ j.acme.2014.12.010.

[9] ABAQUS, 2017, Available: https://www.3ds.com/products-services/simulia/. [Accessed 1 10 2017].

[10] Egyptian Code of Practice (2018), Ministry of Housing.: Utilities and Urban Communities, Egyptian code for design and construction of reinforced concrete structures, E203-2018.

[11] ALTOUBAT, S. – MAALEJ, M. – SHAIKH, F. U. A.: Laboratory Simulation of Corrosion Damage in Reinforced Concrete. International Journal of Concrete Structures and Materials, 10(3), 2016, pp. 383-391.

[12] MOHAMMAD M. KASHANI - LAURA N. LOWES - ADAM J. CREWE - NICHOLAS A. ALEXANDER: Computational Modelling Strategies for Nonlinear Response Prediction of Corroded Circular RC Bridge Piers. Advances in Materials Science and Engineering, Vol. 2016, Article ID 2738265, 15 p., 2016, https://doi.org/10.1155/2016/2738265.

[13] MOHAMMED, A. M. Y. - AHMED, A. - MAEKAWA, K.: Comparative Nonlinear Behavior of Corroded Circular and Square RC Columns. KSCE Journal of Civil Engineering, 24, pp. 2110-2119.

[14] KHALID, N. N.: Strength Reduction of Reinforced Concrete Columns Subjected to Corrosion Related Cover Spalling. Doctoral dissertation, University of Akron.

[15] FANG, L. - ZHOU, Y. - YI, D. - YI, W.: Experimental Study on Flexural Capacity of Corroded RC Slabs Reinforced with Basalt Fiber Textile. Applied Sciences, 11(1), 2021, p. 144.

[16] QIANG LI - XIANYU JIN - DONGMING YAN - CHUANQING FU - JUN XU: Study of Wiring Method on Accelerated Corrosion of Steel Bars in Concrete. https://doi.org/10.1016/j.conbuildmat.2020.121286.

[17] CHARLOTTE VAN STEEN - ELS VERSTRYNGE - MARTINE WEVERS - LUCIE VANDEWALLE: Assessing the Bond Behavior of Corroded Smooth and Ribbed Rebars with Acoustic Emission Monitoring. Cem. Concr. Res. 120, 2019, 176–186.